Resistive Impedance Matching Circuit for Piezoelectric Energy Harvesting

NA KONG,[1,*] DONG SAM HA,[1] ALPER ERTURK[2] AND DANIEL J. INMAN[3]

[1]*Department of Electrical and Computer Engineering, Virginia Tech, Blacksburg, VA 24061, USA*

[2]*Department of Engineering Science and Mechanics, Virginia Tech, Blacksburg, VA 24061, USA*

[3]*Department of Mechanical Engineering, Virginia Tech, Blacksburg, VA 24061, USA*

ABSTRACT: A two-stage power conditioning circuit consisting of an AC–DC converter followed by a DC–DC converter is proposed for a vibration-based energy harvesting system. The power conditioning circuit intends to maximize the amount of power extracted from a piezoelectric energy harvester by matching the source impedance with the circuit by adaptively adjusting the duty cycle. An equivalent electrical circuit representation derived from a distributed-parameter piezoelectric energy harvester model is adapted to enable the impedance matching method proposed here. For a given piezoelectric energy harvester, there is a theoretical maximum power output that is determined by the mechanical damping, base acceleration, and the effective mass of the harvester structure under base excitation. Experimental results are given to validate the effectiveness of the proposed resistive impedance matching circuit around the first resonance frequency of a cantilevered piezoelectric energy harvester.

Key Words: piezoelectric energy harvesting, resistive impedance matching, DC-DC converter.

INTRODUCTION

A variety of wireless and portable applications have emerged in recent years providing convenience and new abilities. However, the batteries used to power such devices add to toxic waste, require repeated maintenance (changing or charging the batteries), and often result in volume requirements exceeding the requirements of some applications (Paradiso and Starner, 2005; Hudak and Amatucci, 2008; Mathuna et al., 2008). Energy harvesting from a variety of ambient sources (heat, solar, wind, vibration, and radio frequency radiation) provide possible solutions (Hagerty et al., 2000; Beeby et al., 2006; Singh et al., 2006; Alippi and Galperti, 2008; Lhermet et al., 2008; Torah et al., 2008). Here we focus on harvesting ambient harmonic vibration using the piezoelectric effect (Anton and Sodano, 2007; Priya, 2007).

Vibration energy harvesting has attracted immense research interest owing to its relatively low cost and high power density. Ambient vibrations are present in various environments, such as automotive vehicles, buildings, structures (e.g., bridges and railways), industrial machines, and household appliances. Mechanical vibration energy can be extracted using a suitable mechanical-to-electrical energy converter (or generator) such as electromagnetic, electrostatic, or piezoelectric transduction devices. A vibration-based power generator converts the mechanical vibration energy into AC electrical power. Since microelectronic devices and rechargeable batteries usually require a DC power supply, a power conditioning circuitry is necessary to rectify the AC power to stable DC power. Typically a power conditioning circuit is sensitive to the efficiency of power extraction. Ottman et al. (2002, 2003) derived the optimal DC voltage required to maximize the power extraction under the direct connection of the load to an AC–DC rectifier of a piezoelectric power generator. They also presented an adaptive solution using the DC–DC converter to achieve automated power optimization. Lefeuvre et al. (2007) proposed to use a sensorless buck-boost converter running in discontinuous conduction mode (DCM) to track the optimal working points of the generator. Badel et al. (2006), Guyomar et al. (2005), Richard et al. (1999), and Xu et al. (2005) developed several conditioning circuits to increase piezoelectric power generation that incorporated electronic switches and inductors to shape the delivered voltage.

A new approach for impedance matching to maximize the power extraction is presented in this article. The piezoelectric power generator model obtained from the distributed-parameter electromechanical solution is employed to study the source impedance characteristics. The power extraction efficiency by the complex conjugate and resistive impedance matching loads are

*Author to whom correspondence should be addressed. E-mail: kongna@vt.edu
Figures 6 and 13–17 appear in color online: http://jim.sagepub.com

1045-389X/10/13 1293–10 $10.00/0 DOI: 10.1177/1045389X09357971
© The Author(s), 2010. Reprints and permissions:
http://www.sagepub.co.uk/journalsPermissions.nav

compared through circuit simulation. Simulation results show that resistive matching could be an acceptable compromise for conditioning circuit design when the vibration frequency is around the resonance frequency band of the piezoelectric power generator. A two-stage conditioning circuit with a rectifier and a buck-boost converter is proposed to adaptively achieve the resistive impedance matching. Experimental results are presented to validate the effectiveness of the resistive impedance matching circuit proposed here.

IMPEDANCE MATCHING

Complex Conjugate Matching

The maximum power transfer occurs for a fixed AC source if the load impedance is the complex conjugate of the source impedance (Jackson, 1959). Consider an AC current source shown in Figure 1, for which $i_S(t) = \sqrt{2} I_S \sin(\omega t)$, the internal impedance is $Z_S = R_S + jX_S$ and the load impedance is $Z_L = R_L + jX_L$.

The average power delivered to the load is:

$$P_o = I_{o,rms}^2 R_L = \left| \frac{Z_S}{Z_S + Z_L} \right|^2 I_S^2 R_L = \frac{R_S^2 + X_S^2}{(R_S + R_L)^2 + (X_S + X_L)^2} I_S^2 R_L. \quad (1)$$

When the load is the complex conjugate of the source impedance or $Z_{L,opt} = R_S - jX_S$, the maximum power is delivered, that is:

$$P_{o,\max} = \frac{R_S^2 + X_S^2}{4R_S} I_S^2, \quad (2)$$

where the maximum power output is determined by the source properties only. The voltage output across the source or the load is called optimal voltage and is obtained as:

$$V_{o,opt} = \frac{Z_S I_S}{Z_S + Z_{L,opt}} Z_{L,opt} = \frac{R_S + jX_S}{R_S + jX_S + R_S - jX_S} I_S (R_S - jX_S) = \frac{R_S^2 + X_S^2}{2R_S} I_S, \quad (3)$$

where the optimal voltage is in phase with the current source.

The same conclusion can be drawn for a voltage source of $v_S(t) = \sqrt{2} V_S \sin(\omega t)$ shown in Figure 2. Then the maximum power delivered to the load and the optimal output current are given by Equations (4) and (5), respectively:

$$P_{o,\max} = \left| \frac{V_S}{Z_S + Z_{L,opt}} \right|^2 R_{L,opt} = \frac{V_S^2}{(R_S + R_S)^2 + (X_S - X_S)^2} R_S = \frac{V_S^2}{4R_S}, \quad (4)$$

$$I_{o,opt} = \frac{V_S}{2R_S}. \quad (5)$$

Resistive Impedance Matching

Although the conjugate matching load extracts the maximum power from the source, a direct impedance matching is usually impractical for piezoelectric energy harvesting due to the requirement of a huge inductor. An alternative and suboptimal approach is to use only a resistive load and try to match the source impedance. The power delivered from a current source to a load resistance of R_L can be given by:

$$P_o = \frac{R_S^2 + X_S^2}{(R_S + R_L)^2 + X_S^2} I_S^2 R_L = \frac{R_S^2 + X_S^2}{R_L + \frac{(R_S^2 + X_S^2)}{R_L} + 2R_S} I_S^2. \quad (6)$$

The optimal load resistance maximizing the power delivery to the load and the optimal power for the resistive load can be obtained from Equations (7) and (8), respectively:

$$R_{L,opt} = \sqrt{R_S^2 + X_S^2}, \quad (7)$$

$$P_{o,\max} = \frac{R_S^2 + X_S^2}{2\left(\sqrt{R_S^2 + X_S^2} + R_S\right)} I_S^2. \quad (8)$$

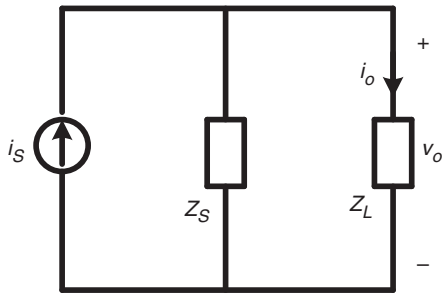

Figure 1. *The circuit with an AC current source.*

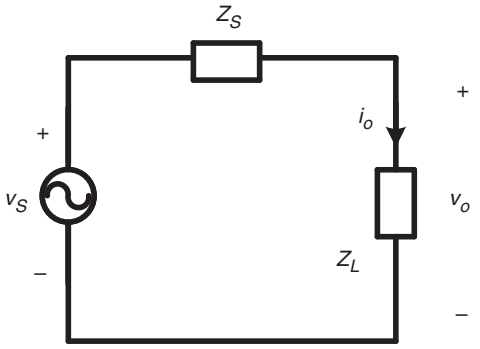

Figure 2. *The circuit with an AC voltage source.*

Clearly, the power delivered to the resistive load (given by Equation (8)) is smaller than the optimal power delivery under the complex conjugate matching (given by Equation (2)). The resistive load matching becomes less efficient for large values of the reactive source component. We adopt the suboptimal resistive load approach, but the efficiency is quite good around the resonant frequency of the system.

INTERNAL IMPEDANCE OF THE PIEZOELECTRIC VIBRATION ENERGY HARVESTER

Electrical Model for Cantilevered Piezoelectric Energy Harvester

The analytical closed-form solution of a cantilevered piezoelectric energy harvester based on distributed-parameter formulation was given by Erturk and Inman (2008a, 2009). Single-mode and multi-mode electrical circuit representations using the Rayleigh–Ritz formulation were presented by Elvin and Elvin (2009) along with verifications against the former analytical solution. The single-mode equivalent circuit based on the Rayleigh–Ritz formulation is shown in Figure 3 for the fundamental mode. The voltage generator $v = m^*a$ represents the effective force induced by the base vibration and is the only source in the electrical model, where m^* is the effective mass term and a is the base acceleration amplitude. The product m^*a is the effective inertia of the cantilever, which is the forcing term in the base excitation problem (Erturk and Inman, 2008b). The equivalent inductance $L = M_{11}$ represents the modal mass of the first mode. The resistance $R = D_{11}$ and the capacitance $C = 1/K_{11}$ represent mechanical damping and compliance (reciprocal of stiffness), respectively. The electromechanical coupling is modeled as a transformer with the turn-ratio n representing the piezoelectric coupling vector. C_p is the equivalent inherent capacitance of the piezoceramic layers. Typically, the leakage resistance of the piezoelectric material is considered in parallel to the inherent capacitance C_p. However, the leakage resistance is normally two orders of magnitude higher than the impedance obtained without taking it into account. Therefore, the effect of the leakage resistance on the overall impedance is neglected in the electrical circuit as done by Erturk and Inman (2008a, 2009) and Elvin and Elvin (2009), among others. This model decouples the mechanical and electrical systems, which enables us to predict electrical output with different loading conditions and to optimize the power conditioning circuit.

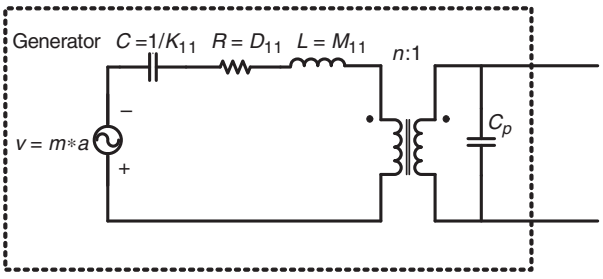

Figure 3. *The equivalent circuit for the first mode piezoelectric generator.*

The piezoelectric generator can be represented as Norton or Thévenin equivalent circuits as shown in Figure 4. The current source i_S in Figure 4(a) is the short-circuit output current, and the voltage source v_S in Figure 4(b) is the open-circuit output voltage.

To calculate the internal impedance Z_S of the generator, we can replace the current source with open circuit and the voltage source with short circuit. The internal impedance Z_S of the generator then can be represented as shown in Figure 5, where:

$$L_S = \frac{L}{n^2} = \frac{M_{11}}{n^2}; \quad R_S = \frac{R}{n^2} = \frac{D_{11}}{n^2};$$
$$C_{S1} = n^2 C = \frac{n^2}{K_{11}}; \quad C_{S2} = C_p. \tag{9}$$

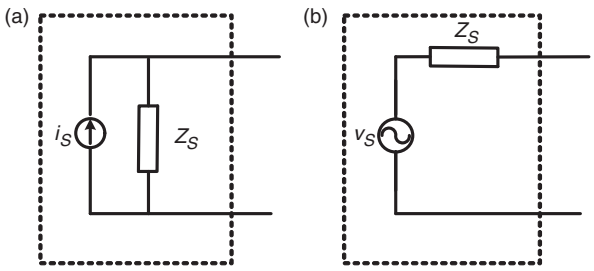

Figure 4. *The simplified generator model: (a) Norton equivalent, (b) Thévenin equivalent.*

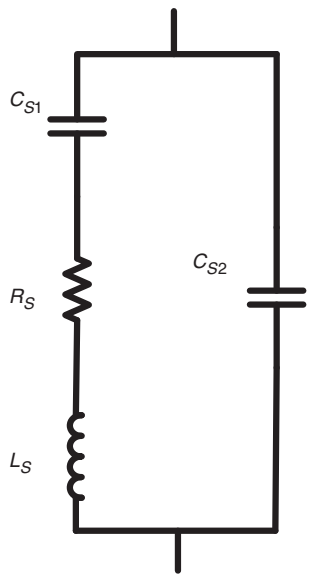

Figure 5. *Equivalent internal impedance Z_S of a piezoelectric generator.*

Case Study

As an example, the bimorph piezoelectric generator used by Erturk and Inman (2009) is presented and has the properties listed in Table 1. The impedance and admittance curves plotted using these properties are shown in Figure 6. The open-circuit resonance frequency f_{oc} of a piezoelectric generator is the frequency which makes the output voltage maximum as the load resistance tends to be infinity (open-circuit condition). In contrast, the short-circuit resonance frequency f_{sc} is one that makes the output current maximum as the load resistance tends to be zero (short-circuit condition). In other words, the open-circuit resonance frequency corresponds to the frequency where the resistance component of the impedance is the maximum. The open-circuit resonance frequency is 48.2 Hz in Figure 6(a). Likewise the short-circuit resonance frequency corresponds to the frequency where the conductance component of the admittance is the maximum and is 45.7 Hz in Figure 6(b).

From Figure 6(a), the source impedance is purely resistive around 47 Hz, where resistance matching can be used to extract maximum power. The source can be approximated as a series of a resistor and a capacitor at other frequencies, and a series of a resistor and an inductor can match the source as shown in Figure 7. For the specific generator under a constant base acceleration level 0.5 g (rms), the required matching load impedances for different vibration frequencies are calculated. The open-circuit output voltage $V_{oc,peak}$ and the average power P_o dissipated by the resistor are obtained through circuit simulations. The results are tabulated in Table 2.

As can be seen from the table, under the same base acceleration level, the theoretical maximum power delivered from a given piezoelectric power generator is constant with respect to different base vibration frequencies. It can be deduced from Equation (4) that the maximum power depends only on the source voltage and the internal resistance. The theoretical maximum power delivered from a given piezoelectric generator is computed as:

$$P_{o,\max} = \frac{V^2}{4R} = \frac{(m^* a_{rms})^2}{4D_{11}} = \frac{(0.1286161 \times 0.5 \times 9.8)^2}{4 \times 15.5061} = 6.4\text{mW}. \quad (10)$$

Therefore, to increase the output power, the generator should be designed to have less mechanical damping to

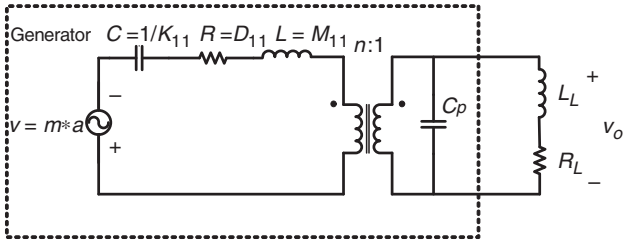

Figure 7. *Piezoelectric generator connected with a matching load.*

Table 1. Modal parameters of the bimorph piezoelectric harvester.

M_{11}	D_{11}	K_{11}	n	C_p	m^*
1	15.50671	82461.67	−0.01964044	41.24e−9	0.1286161

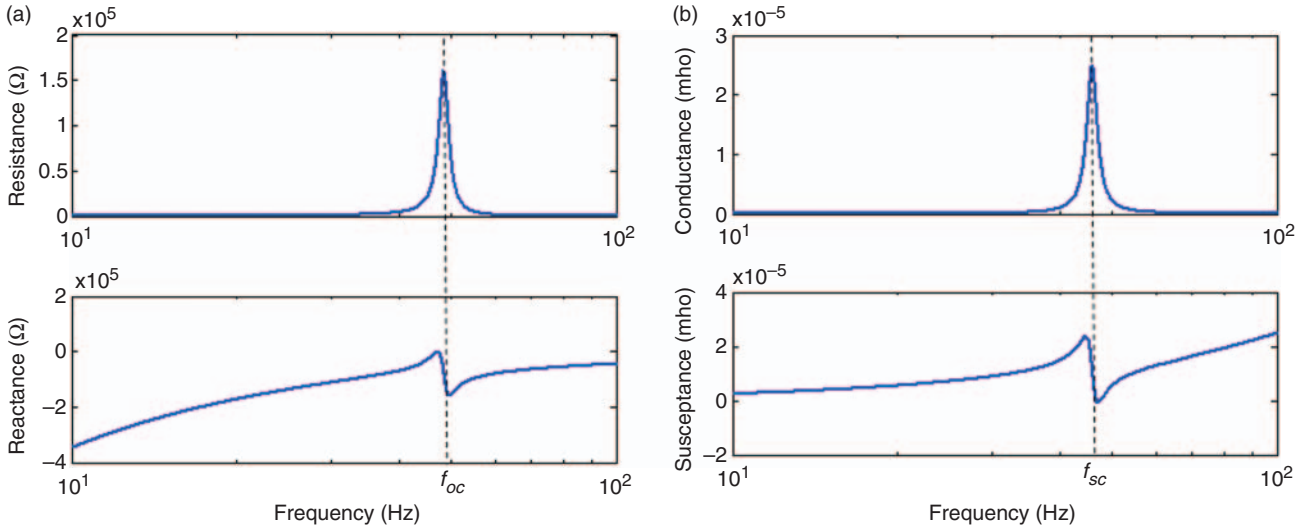

Figure 6. *Internal impedance and admittance of a loaded bimorph piezoelectric harvester: (a) impedance, (b) admittance.*

reduce the internal resistance R in Figure 7. As long as the operation does not cause any damage, large base accelerations and large effective mass (which will result in large effective forcing) are preferable to harvest larger power.

Table 2 shows that the complex conjugate matching load is required to have tens of or even several hundreds of henries inductance, even around the generator's resonance frequency, which makes the conjugate impedance matching impractical. When a resistive impedance matching is employed, the output power can only be a fraction of the theoretical maximum power. The power harvesting efficiency is around 75% between the short-circuit and the open-circuit resonance frequencies. However, the efficiency drops off sharply outside the frequency range. Therefore, the resistive impedance matching is an acceptable compromise, provided that the resonance frequency band of the harvester is tuned to the excitation frequency. In the following, we propose a circuit design method with adjustable input impedance to realize resistive impedance matching.

Review of Existing Resistive Impedance Matching Methods

As described in the above section, resistive matching can be quite effective between the short-circuit and the open-circuit resonance frequencies of a generator. Hence, if the load resistance value can be changed adaptively to match the source impedance, high power extraction efficiency can be achieved in the short-to-open resonance frequency band.

Researchers (Ottman et al., 2002, 2003; Lefeuvre et al., 2007) have considered using a two-stage conditioning circuit to effectively realize resistive impedance matching as shown in Figure 8. The first stage is an AC–DC rectifier and the following stage is a switching mode DC–DC converter providing DC output to the ultimate load. An electrolytic capacitor, which is usually bulky, is located in-between to smooth the output voltage of the first stage.

Ottman et al. (2002, 2003) presented an approach using buck converter as the second stage for power conditioning and the optimal rectified voltage was derived to maximize the power delivery. However, the buck converter can only work when the input voltage is higher than its output voltage, which limits the application of the circuit to vibration harvesters generating voltage higher than the output voltage. For example, for piezoelectric power generators excited by low-level acceleration, buck converters cannot be used directly due to low voltage output from the device. Such converters are also inefficient for electromagnetic energy harvesting where the voltage output is typically low.

A DC–DC converter should be able to step up or step down the input voltage, so it can be applied for a wide range of energy harvesters. Some traditional DC–DC converters can provide this, such as buck-boost, flyback, and Sepic converters. Also importantly, these converters operating in DCM mode behave as resistors (Erickson and Maksimovic, 2001). A buck-boost converter requires a smaller number of components compared with flyback and Sepic converters and hence less complex. Lefeuvre et al. (2007) proposed to use DCM buck-boost converter functioning as a matched resistance. In order to reduce the power consumption of the control circuit, a low-power crystal clock with a fixed duty cycle and a fixed frequency was used to drive the power switch for their circuit. Unfortunately, it makes the circuit less flexible for various piezoelectric generators and limits on the output voltage of the generator due to a limited voltage range of the crystal clock.

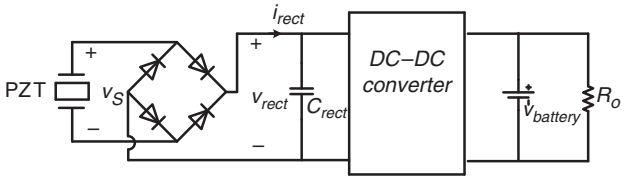

Figure 8. *Existing resistive impedance matching circuit.*

Table 2. Simulation results with matching load impedance.

	Conjugate matching			Resistive matching		
Frequency (Hz)	$V_{oc,peak}$ (V)	R_L (kΩ)	L_L (H)	P_o (mW)	R_L (kΩ)	P_o (mW)
44.0	26.6	13.9	137.6	6.40	40.6	3.24
45.0	33.5	22.5	90.8	6.40	34.3	5.00
45.7	41.3	32.8	54.2	6.40	36.2	6.04
46.0	45.1	39.4	37.2	6.40	41.1	6.29
47.0	65.2	83.2	0	6.40	83.2	6.40
48.0	89.0	157.2	191.4	6.40	164.2	6.23
48.2	90.3	159.4	254.5	6.40	177.1	6.05
49.0	75.7	106.5	486.2	6.40	185.2	4.81
50.0	50.1	50.7	469.8	6.40	155.2	3.10

Proposed Resistive Impedance Matching Circuit

A buck-boost converter running in DCM directly preceded by a rectifier shown in Figure 9 is proposed in this article. Unlike previous approaches (Ottman et al., 2002, 2003; Lefeuvre et al., 2007), the big smoothing capacitor right after the rectifier, i.e., C_{rect} in Figure 8 is eliminated. A low-power oscillator circuit drives the power switch. The duty cycle and the frequency of the oscillator can be adjusted in a wide range to match the source impedance. The voltage and current waveforms during one period of a harmonic base vibration are shown in Figure 10.

Since the base vibration frequency is much slower than the designed switching frequency F_S, the rectified voltage or the input voltage of the buck-boost converter can be treated as DC during a switching period T_S. The voltage and current waveforms during one switching period are shown in Figure 11.

For simplicity, the power switch, diodes, and LC filters are assumed to be lossless. The derivation considering the losses in the electrical components is included in the Appendix. The effective input resistance of a DCM buck-boost converter is given by Erickson and Maksimovic (2001) as:

$$R_{in} = \frac{v_{rect}}{\frac{1}{T_S}\int_0^{D_1 T_S} i_L \mathrm{d}t} = \frac{v_{rect}}{\frac{1}{T_S}\int_0^{D_1 T_S} \frac{v_{rect}}{L} t \mathrm{d}t} = \frac{v_{rect}}{\frac{1}{T_S}\frac{v_{rect}}{L}\frac{(D_1 T_S)^2}{2}} = \frac{2L}{D_1^2 T_S} \tag{11}$$

In order to achieve the resistive impedance matching, the effective input resistance R_{in} should be equal to the optimal resistive load $R_{in,opt}$ given in Equation (7). Hence, the optimal duty cycle can be expressed as:

$$D_{1,opt} = \sqrt{\frac{2L}{R_{in,opt} T_S}}. \tag{12}$$

Once the inductance value and the switching frequency are chosen, the duty cycle for the maximum output power can be obtained. In the proposed circuit,

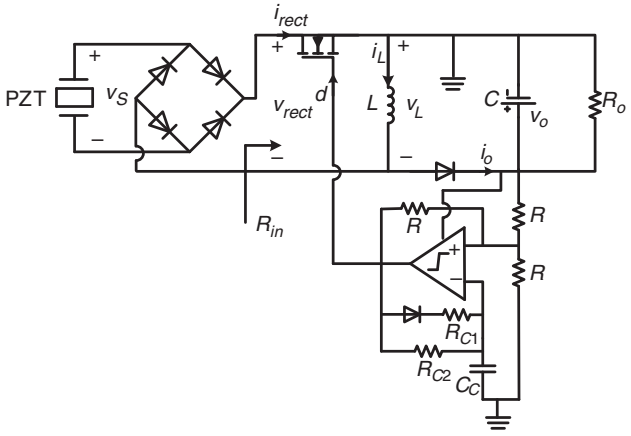

Figure 9. *Proposed resistive impedance matching circuit.*

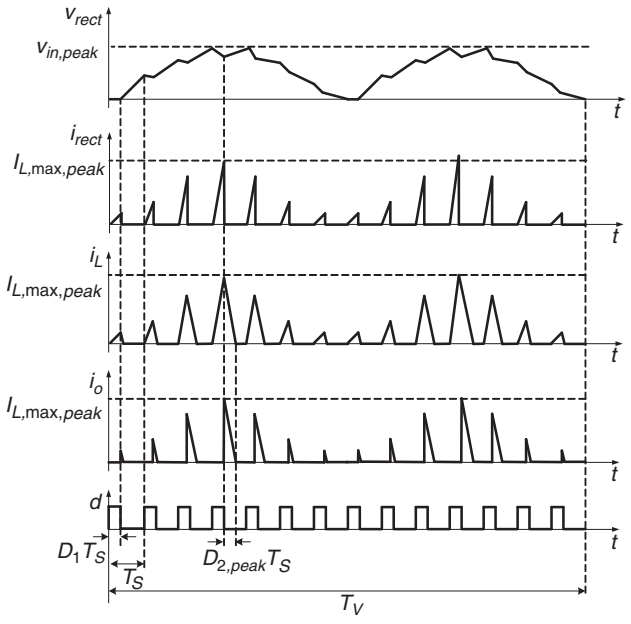

Figure 10. *Waveforms during one period of a harmonic base vibration.*

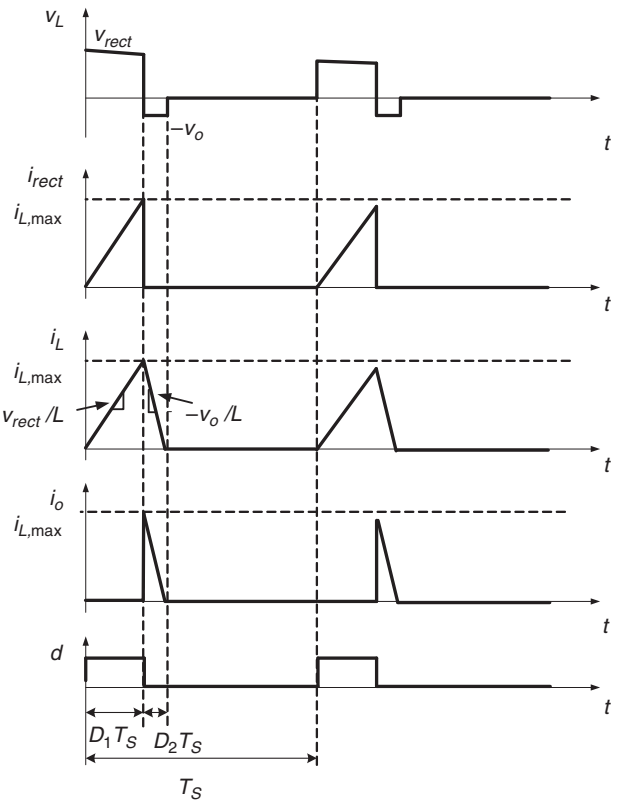

Figure 11. *Waveforms during one switching period.*

a low-power comparator with an RC network is used to generate the gate signal driving the power switch. The duty cycle and switching frequency can be tuned by the R_{C1}, R_{C2}, and C_C (Paing et al., 2008) in Figure 9. The voltage waveforms of the comparator's output and two input nodes are shown in Figure 12.

If the comparator output is high, i.e., equal to the supply voltage (v_o in the proposed circuit in Figure 9), the voltage at the non-inverting input of the comparator is two-thirds of the supply voltage. Capacitor C_C is charged through parallel R_{C1} and R_{C2}. Once the capacitor voltage reaches two-thirds of the supply voltage, the comparator output goes low, i.e., the ground voltage. The voltage at the non-inverting input of comparator is now one-third of the supply voltage. Capacitor C_C is discharged through R_{C2}. Once the capacitor voltage reaches one-third of the supply voltage, the comparator output becomes high and the entire cycle repeats. If R_{C2} is chosen to be much larger than R_{C1}, the duty cycle and the frequency are approximately as follows:

$$D_1 \approx \frac{R_{C1}}{R_{C2}}, \tag{13}$$

$$F_S \approx \frac{1}{(R_{C1} + R_{C2})C_C \ln 2}. \tag{14}$$

EXPERIMENTAL RESULTS

To verify the feasibility of the proposed resistive impedance matching circuit, experiments were performed using a cantilevered bimorph generator with a tip mass. The experimental setup is shown in Figure 13.

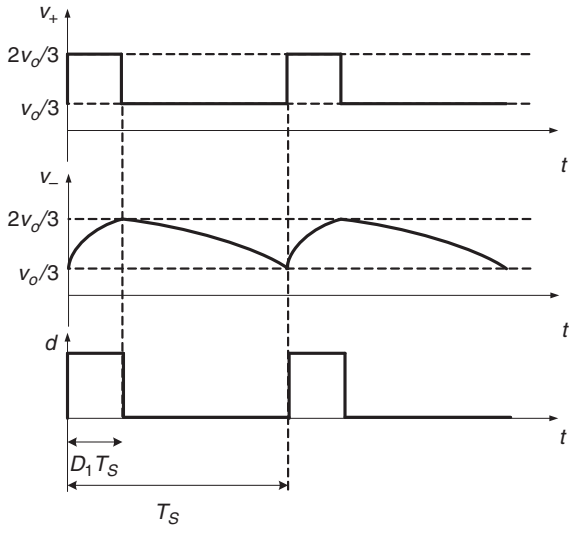

Figure 12. *Waveforms of the output and two input nodes of the comparator.*

The bimorph (manufactured by Piezo Systems, Inc. with model number T226-A4-503X) consists of two oppositely poled PZT-5A piezoelectric elements bracketing a brass substructure layer, and the two piezoelectric elements are connected in series.

The electromechanical frequency response functions (FRFs) that relate the tip velocity to the base acceleration were measured to obtain the short-circuit and open-circuit resonance frequencies of the cantilevered bimorph generator, and the measurement results are shown in Figure 14. The short-circuit and open-circuit resonance frequencies are 53.0 and 56.1 Hz, respectively. The external load resistance was tuned based on real power output to find the optimal resistive load of the piezoelectric energy harvester around the resonance frequency, and the result is shown in Figure 15. The optimal resistive load is in the range of 20–120 kΩ.

The next step is to decide the component values of the buck-boost converter and circuit parameters including

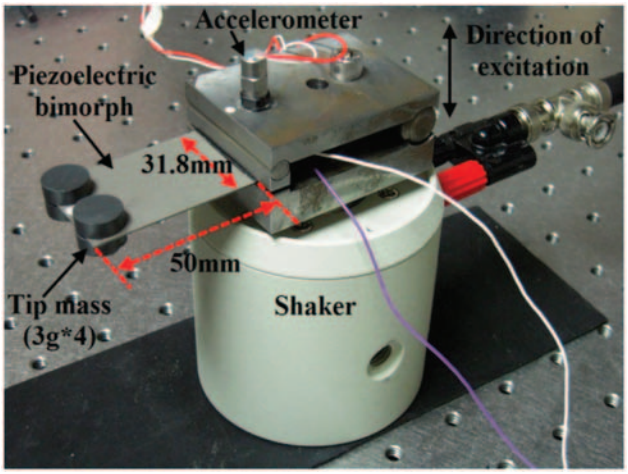

Figure 13. *Cantilevered bimorph generator.*

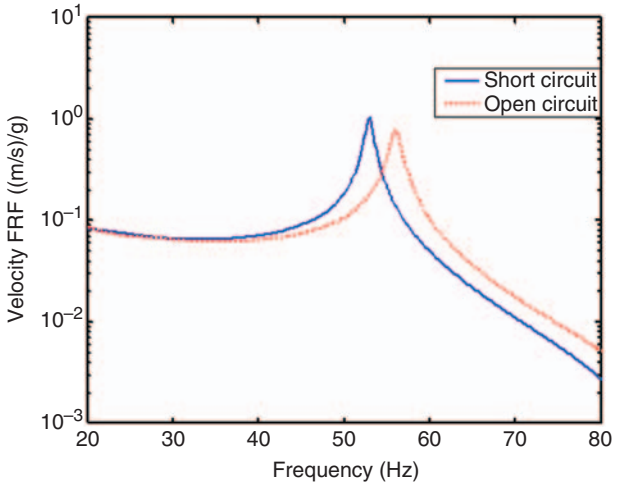

Figure 14. *Short-circuit and open-circuit velocity FRFs of the energy harvester.*

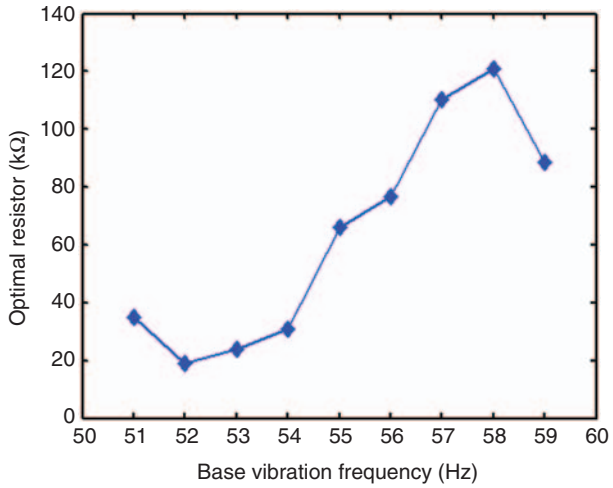

Figure 15. *Optimal resistance versus excitation frequency.*

the switching frequency. The switching frequency should be much higher than the base vibration frequency to manipulate the shape of the generator's voltage output; on the other side, a higher switching frequency causes higher switching loss on the power switch and the diode. We chose the switching frequency of 1 kHz, around 20 times of the excitation frequency, which is not necessary optimal, but sufficient for a proof of the concept. A larger inductor causes smaller current ripple and therefore smaller rms current and conduction loss. However, a larger inductor is bulkier and has larger parasitic resistance to result in higher conduction loss. We chose a 1 mH inductor. Other components were selected based on the voltage and current stresses. For the experiment, the harvester is designed to be excited under the rms acceleration amplitude of 0.5 g. The voltage and current stresses are around 30 V and 200 mA, respectively. The components used in the experiment are listed in Table 3.

The duty cycle and the switching frequency were tuned by choosing appropriate R_{C1}, R_{C2}, and C_C to achieve the maximum power delivery. The optimal duty cycle values around the resonance frequency tuned in the experiment are shown in Figure 16 against the expected values from Equation (12). The experimental results closely match the theoretical trend and the optimal value. The average power harvested by the proposed circuit is plotted in Figure 17 along with the average power harvested directly by the optimal resistive load (shown in Figure 15).

The power harvested by the proposed circuit is in the range of 1.0–3.5 mW around the resonance frequency for an rms base acceleration amplitude of 0.5 g. According to Figure 17, the overall power harvesting efficiency of the proposed circuit is 58–72% of the available power extracted by the optimal resistive loads. The power dissipation in the circuit is mainly due to the conduction loss of the diode and the inductor.

Table 3. Components used in the proposed circuit.

Component	Part number	Notes
Rectifier	BAS3007	$V_F = 0.35$ V at 100 mA
MOSFET	2N7002	$R_{dson} = 1.7\ \Omega$; $C_{iss} = 20$ pF, $C_{oss} = 11$ pF
Schottky Diode	PMEG4005	$V_F = 0.295$ V at 10 mA
Inductor	SL2125-102K1R3	$L = 1.0$ mH; DCR = 0.35 Ω.
Supercapacitor	GW209F	$C = 0.12$ F; ESR = 70 mΩ.
Comparator	TLV3419	$I_q = 0.85$ μA at 5 V

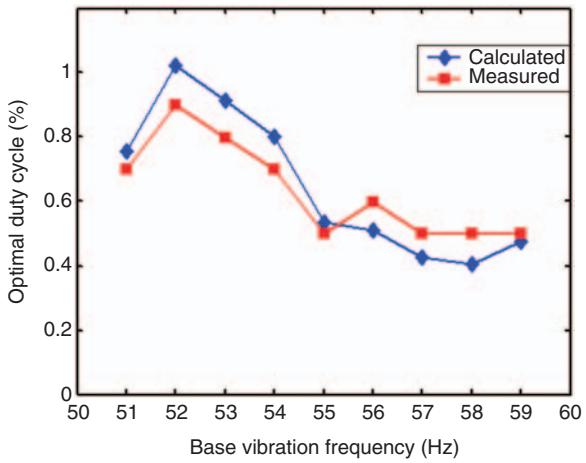

Figure 16. *The optimal duty cycle of the proposed circuit versus excitation frequency.*

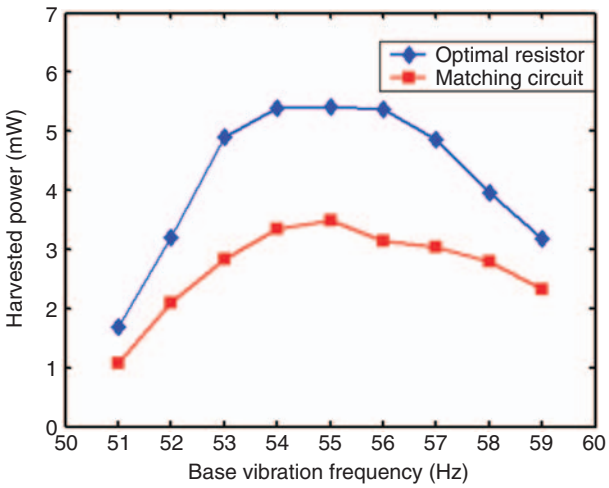

Figure 17. *Harvested power of the proposed circuit.*

CONCLUSIONS AND FUTURE WORK

A resistive impedance matching circuit for piezoelectric energy harvesting is presented in this article. An equivalent electrical model of a piezoelectric

generator based on the distributed-parameter formulation is used to implement the impedance matching. For a given piezoelectric energy harvester, there is a theoretical maximum power output which is determined by the mechanical damping, base acceleration and the effective mass (which yields the effective forcing under base excitation). Due to the impracticality of a large inductance for conjugate impedance matching, we used a buck-booster converter to adaptively match the source impedance of piezoelectric harvester in the short-circuit to open-circuit resonance frequency range of the harvester. Our experiment shows that the proposed circuit can harvest 58–72% of the available power around the fundamental resonance of the harvester.

Future work will consider designing a high-speed and low-power consumption feedback controller to automatically tune the duty cycle to achieve impedance matching. A careful loss analysis will help to choose appropriate components. Adoption of synchronous switching techniques is also promising to further improve the power harvesting efficiency when the resonance of the energy harvesting device is not well tuned to the vibration frequency.

ACKNOWLEDGMENTS

The authors gratefully acknowledge the support of the Air Force Office of Scientific Research MURI under grant number F 9550-06-1-0326 "Energy Harvesting and Storage Systems for Future Air Force Vehicles" monitored by Dr. B. L. Lee and that of the U.S. Department of Commerce, National Institute of Standards and Technology, Technology Innovation Program, Cooperative Agreement Number 70NANB9H9007, USA.

APPENDIX

When the losses of the electrical components are considered, the switch current or the inductor current waveform during the switch on-time ($0 \sim D_1 T_S$) in Figure 11 is not a straight line with a slope of v_{rect}/L, but can be described as:

$$L\frac{\mathrm{d}i_L}{\mathrm{d}t} = v_{rect} - i_L(R_{dson} + R_{dcr}) \quad \text{for} \quad 0 \le t \le D_1 T_S, \quad \text{(A1)}$$

where R_{dson} is the resistance of MOSFET during on-time and R_{dcr} is the parasitic resistance of the inductor. It can readily be obtained that:

$$i_L = \frac{v_{rect}}{R_{dson} + R_{dcr}}\left[1 - \exp\left(-\frac{R_{dson} + R_{dcr}}{L}t\right)\right] \quad \text{for} \quad 0 \le t \le D_1 T_S. \quad \text{(A2)}$$

Then the effective input resistance of the buck-boost converter becomes:

$$\begin{aligned} R_{in} &= \frac{v_{rect}}{\frac{1}{T_S}\int_0^{D_1 T_S} i_L \mathrm{d}t} \\ &= \frac{v_{rect}}{\frac{1}{T_S}\int_0^{D_1 T_S} \frac{v_{rect}}{R_{dson}+R_{dcr}}\left[1 - \exp\left(-\frac{R_{dson}+R_{dcr}}{L}t\right)\right]\mathrm{d}t}. \\ &= \frac{T_S(R_{dson} + R_{dcr})}{D_1 T_S + \frac{L}{R_{dson}+R_{dcr}}\left[\exp\left(-\frac{R_{dson}+R_{dcr}}{L}D_1 T_S\right) - 1\right]} \end{aligned} \quad \text{(A3)}$$

where D_1 can be computed numerically. The equation can be further simplified by using Taylor series expansion of the exponential function, i.e., $\exp(x) \approx 1 + x + x^2/2$ for $|x| << 1$. Therefore, Equation (A3) can be reduced to:

$$\begin{aligned} R_{in} &\approx \frac{T_S(R_{dson} + R_{dcr})}{D_1 T_S + \frac{L}{R_{dson}+R_{dcr}}\left(\frac{R_{dson}+R_{dcr}}{L}D_1 T_S + \frac{((R_{dson}+R_{dcr})D_1 T_S)^2}{2L^2}\right)} \\ &= \frac{2L}{D_1^2 T_S}. \end{aligned} \quad \text{(A4)}$$

Here, the third and higher order terms of the Taylor series are neglected provided:

$$\frac{R_{dson} + R_{dcr}}{L} D_1 T_S << 1. \quad \text{(A5)}$$

Note that Equations (A4) and (11) are identical. By substituting Equation (12) into (A5), we obtain Equation (A6), which is the assumption of Equation (A4) in practice:

$$(R_{dson} + R_{dcr})\sqrt{\frac{2T_S}{R_{in,opt}L}} << 1. \quad \text{(A6)}$$

It should also be noticed that v_{rect} is canceled out in Equation (A3), i.e., the input impedance of the DCM buck-boost converter is not a function of the input voltage. Therefore, even though there is a finite voltage drop on the conducting diodes of the rectifier, it will not affect the impedance matching between the piezoelectric generator and the interface circuit. Other losses such as the voltage drop of conducting diode connected to the output capacitor and the parasitic resistance of output capacitance will not affect the impedance matching either.

In summary, if the circuit parameters satisfy the inequality given by Equation (A6), the duty cycle D_1 of the power switch can simply be calculated using Equation (12). However, if the inequality given by Equation (A6) cannot be satisfied, the duty cycle D_1 should be solved from Equation (A3).

Using Equation (12) will result in impedance mismatch as well as power losses.

REFERENCES

Alippi, C. and Galperti, C. 2008. "An Adaptive System for Optimal Solar Energy Harvesting in Wireless Sensor Network Nodes," *IEEE Transactions on Circuits and Systems I: Regular Papers*, 55:1742–1750.

Anton, S.R. and Sodano, H.A. 2007. "A Review of Power Harvesting Using Piezoelectric Materials (2003–2006)," *Smart Materials and Structures*, 16:R1–R21.

Badel, A., Benayad, A., Lefeuvre, E., Lebrun, L., Richard, C. and Guyomar, D. 2006. "Single Crystals and Nonlinear Process for Outstanding Vibration-powered Electrical Generators," *IEEE Transactions on Ultrasonics, Ferroelectrics, and Frequency Control*, 53: 673–684.

Beeby, S.P., Tudor, M.J. and White, N.M. 2006. "Energy Harvesting Vibration Sources for Microsystems Applications," *Measurement Science & Technology*, 17:R175–R195.

Elvin, N.G. and Elvin, A.A. 2009. "A General Equivalent Circuit Model for Piezoelectric Generators," *Journal of Intelligent Material Systems and Structures*, 20: 3–9.

Erickson, W. and Maksimovic, D. 2001. *Fundamentals of Power Electronics*, 2nd edn, Kluwer Academic Publishers, Norwell, MA.

Erturk, A. and Inman, D.J. 2008a. "A Distributed Parameter Electromechanical Model for Cantilevered Piezoelectric Energy Harvesters," *Journal of Vibration and Acoustics*, 130(4):041002.1–041002.15.

Erturk, A. and Inman, D.J. 2008b. "Issues in Mathematical Modeling of Piezoelectric Energy Harvesters," *Smart Materials and Structures*, 17:065016.

Erturk, A. and Inman, D.J. 2009. "An Experimentally Validated Bimorph Cantilever Model for Piezoelectric Energy Harvesting from Base Excitations," *Smart Materials and Structures*, 18(2):025009.1–025009.18.

Guyomar, D., Badel, A., Lefeuvre, E. and Richard, C. 2005. "Toward Energy Harvesting Using Active Materials and Conversion Improvement by Nonlinear Processing," *IEEE Transactions on Ultrasonics, Ferroelectrics and Frequency Control*, 52:584–595.

Hagerty, J.A., Lopez, N.D., Popovic, B. and Popovic, Z. 2000. "Broadband Rectenna Arrays for Randomly Polarized Incident Waves," In: *European Microwave Conference*, October 2000, France, Paris, pp. 1–4.

Hudak, N.S. and Amatucci, G.G. 2008. "Small-Scale Energy Harvesting Through Thermoelectric, Vibration, and Radiofrequency Power Conversion," *Journal of Applied Physics*, 103:101301.

Jackson, H.W. 1959. *Introduction to Electronic Circuits*, Prentice-Hall, Englewood Cliffs, New Jersey.

Lefeuvre, E., Audigier, D., Richard, C. and Guyomar, D. 2007. "Buck-Boost Converter for Sensorless Power Optimization of Piezoelectric Energy Harvester," *IEEE Transactions on Power Electronics*, 22:2018–2025.

Lhermet, H., Condemine, C., Plissonnier, M., Salot, R., Audebert, P. and Rosset, M. 2008. "Efficient Power Management Circuit: From Thermal Energy Harvesting To Above-IC Microbattery Energy Storage," *IEEE Journal of Solid-State Circuits*, 43:246–255.

Mathuna, C.O., O'Donnell, T., Martinez-Catala, R.V., Rohan, J. and O'Flynn, B. 2008. "Energy Scavenging for Long-term Deployable Wireless Sensor Networks," *Talanta*, 75(3):613–623.

Ottman, G.K., Hofmann, H.F., Bhatt, A.C. and Lesieutre, G.A. 2002. "Adaptive Piezoelectric Energy Harvesting Circuit for Wireless Remote Power Supply," *IEEE Transactions on Power Electronics*, 17:669–676.

Ottman, G.K., Hofmann, H.F. and Lesieutre, G.A. 2003. "Optimized Piezoelectric Energy Harvesting Circuit Using Step-down Converter in Discontinuous Conduction Mode," *IEEE Transactions on Power Electronics*, 18:696–703.

Paing, T., Shin, J., Zane, R. and Popovic, Z. 2008. "Resistor Emulation Approach to Low-Power RF Energy Harvesting," *IEEE Transactions on Power Electronics*, 23:1494–1501.

Paradiso, J.A. and Starner, T. 2005. "Energy Scavenging for Mobile and Wireless Electronics," *IEEE Pervasive Computing*, 4:18–27.

Priya, S. 2007. "Advances in Energy Harvesting Using Low Profile Piezoelectric Transducers," *Journal of Electroceramics*, 19:165–182.

Richard, C., Guyomar, D., Audigier, D. and Ching, G. 1999. "Semi-passive Damping Using Continuous Switching of a Piezoelectric Device," In: *Proceedings of SPIE Smart Structures and Materials Conference*, Vol. 3672, pp. 104–111, Newport Beach, CA.

Singh, P., Kaneria, S., Anugonda, V.S., Chen, H.M., Wang, X.Q., Reisner, D.E. and LaFollette, R.M. 2006. "Prototype Silicon Micropower Supply for Sensors," *IEEE Sensors Journal*, 6:211–222.

Torah, R., Glynne-Jones, P., Tudor, M., O'Donnell, T., Roy, S. and Beeby, S. 2008. "Self-powered Autonomous Wireless Sensor Node Using Vibration Energy Harvesting," *Measurement Science & Technology*, 19:125202.

Xu, S., Ngo, K.D.T., Nishida, T., Gyo-Bum, C. and Sharma, A. 2005. "Converter and Controller for Micro-power Energy Harvesting," *IEEE Applied Power Electronics Conference and Exposition*, 1:226–230.